

**INVESTIGATION OF HADRON MULTIPLICITIES AND HADRON YIELD RATIOS IN HEAVY ION COLLISIONS**

**D.R. OLIINYCHENKO,<sup>1</sup> K.A. BUGAEV,<sup>2</sup> A.S. SORIN<sup>1</sup>**

<sup>1</sup>**Bogoliubov Laboratory of Theoretical Physics**  
*(6, Joliot-Curie Str., JINR, Dubna 141980, Russia; e-mail: dimafopf@gmail.com)*

<sup>2</sup>**Bogolyubov Institute for Theoretical Physics, Nat. Acad. of Sci. of Ukraine**  
*(14b, Metrolohichna Str., Kyiv 03680, Ukraine; e-mail: bugaev@th.physik.uni-frankfurt.de)*

PACS 25.75.-q, 25.75.Nq  
 ©2013

arXiv:1204.0103v2 [hep-ph] 17 Apr 2014

Here we thoroughly discuss some weak points of the thermal model which is traditionally used to describe the hadron multiplicities measured in the central nucleus-nucleus collisions. In particular, the role of conservation laws, the values of hard-core radii along with the effects of the Lorentz contraction of hadron eigen volumes and the hadronic surface tension are systematically studied. It is shown that for the adequate description of hadron multiplicities the conservation laws should be modified, whereas for the description of hadron yield ratios the conservation laws are not necessary at all. Also here we analyzed the usual criteria for the chemical freeze-out and found that none of them is robust. A new chemical freeze-out criterion of constant entropy per hadron equals to 7.18 is suggested and a novel effect of adiabatic chemical hadron production is discussed. Additionally, we found that the data for the center of mass energies above 10 GeV lead to the temperature of the nil hadronic surface tension coefficient of about  $T_0 = 147 \pm 7$  MeV. This is a very intriguing result since a very close estimate for such a temperature was obtained recently within entirely different approach. We argue that these two independently obtained results evidence that the (tri)critical temperature of the QCD phase diagram is between 140 and 154 MeV. In addition, here we suggest to consider the pion and kaon hard-core radii as new fitting parameters. Such an approach for the first time allows us to simultaneously describe the hadron multiplicities and the Strangeness Horn and get a very high quality fit of the available experimental data.

**1. Introduction**

Experimental data on heavy ion collisions has traditionally been described by the thermal model [1-27]. The thermal model core assumption is that fireball produced in the relativistic nuclear collision reaches thermodynamic equilibrium. Such an assumption allows one to describe the multiplicities of particles registered in the experiment using two parameters, namely the tempera-

ture  $T$  and baryo-chemical potential  $\mu_b$ . The extracted values of  $T$  and  $\mu_b$  not only describe the experimental data, but they also give an essential information about the last stage of fireball evolution, when the inelastic collisions cease to exist, but the elastic collisions between hadron and the decay of resonances take place. This stage is usually called the chemical freeze-out. The thermal model was initially used for the AGS and SPS data [13] and was subsequently employed to describe the data collected at SIS [14, 15], SPS [16] and RHIC [17-20]. Using the thermal model it was possible to correctly predict the hadron ratios measured at LHC [2], while the only wrong prediction for LHC was made for  $\bar{p}/\pi^-$  ratio [21]. An analysis of the energy dependence of thermal parameters extracted from fits of the experimental data established the line of chemical freeze-out [22]. Consequently, thermal model is an established tool for particle production analysis and chemical freeze-out investigation.

However, the thermal model suffers from several weak points which should be accounted for in more careful studies. The present paper is just devoted to a critical analysis of the thermal model and contains several directions to develop and improve it. First of all we would like to notice that the term "thermal model" is a common name for a set of similar models, each having its specific features such as the strangeness suppression factor  $\gamma_s$ , the inhomogeneous freeze-out scenario [14, 19, 26, 27] etc. Here we consider the minimal thermal model with two major parameters  $T$  and  $\mu_b$ , following the approach of Andronic et al., [2], and below we briefly formulate the main problems of the model to be analyzed in the present work.

- **Particle table.** In order to describe the experimental data using the thermal model one needs the masses, the widths and the decay branching ratios of all existing resonances. In principle, the mass spectrum of the hadronic resonances that are heavier than 2,3 GeV is known poorly and, hence, they could create a problem. However, recently it was shown that the large width of heavy resonances leads to their strong suppression [28] and, hence, their contribution into the thermodynamic functions of hadronic phase is negligible.

Note that not only the parameters of hadrons from the "tail" of mass spectrum are poorly known. For example, both the mass and the width of  $\sigma(600)$  meson are not well established, but the thermal model predictions are strongly influenced by the values of the mass and width of this meson [3], while for many other baryons the width and branching ratios of decays are not well established at all. Thus, the particle table is one source of uncertainty of the thermal model.

- **Hard-core spheres radii value.** The ideal gas description has proven to be unsatisfactory [4] long ago. The simplest way to introduce an interaction between hadrons is to use the repulsive hard-core potential, since the attraction between them is usually accounted for via many sorts of hadrons [28]. In the simplest case this potential depends only on a single parameter - the hard-core radius. In general case, each particle type may have its own hard-core radius. But for the sake of convenience and simplicity the hard-core radius is usually taken equal for all particles. The usual value for such a radius is  $r = 0.3$  fm. This value is motivated by the hard-core volume known from nucleon-nucleon scattering [1]. There are, however, two restrictions on the hard-core radii range: (i) they should be small enough to satisfy the condition  $V_{eigen} \ll V$ , i.e. that the total eigen volume of all particles  $V_{eigen}$  should be much smaller than total volume of the system  $V$ ; (ii) on the other hand, these radii shouldn't be too small, because otherwise the model will lead to a contradiction with the lattice quantum chromodynamics (QCD) thermodynamics data [8]. Thus, there is a certain freedom in defining the hard-core radii values which, so far, was not systematically exploit to describe the whole massive of existing experimental data.

- **Conservation laws.** Also here we would like to discuss the baryon charge and isospin projection conservation laws. It was suggested to use them in the form [2]

$$\begin{cases} \sum_i n_i I_{3i} = I_{3init}/V, \\ \sum_i n_i B_i = B_{init}/V. \end{cases}$$

The initial values are chosen  $I_{3init} = -20$  and  $B_{init} = 200$  [2], neglecting the fact that only the part of initial particles belong to the midrapidity region. Below we study the role of these conservation laws and show that such a treatment leads to physically unrealistic freeze-out volumes and to very bad description of hadron multiplicities, while the particle yield ratios (we use such a term for the ratio of multiplicities in order avoid a confusion) description can be extremely good.

- **Multiplicities fit.** The fit of hadron multiplicities is usually performed using three parameters:  $T$ ,  $\mu_b$ , and  $V$  [2]. Below we show that such a procedure combined with above mentioned conservation laws is mathematically ambiguous and it leads to the problems with the imposed baryonic charge conservation law.

In addition to these usual features of the thermal model we would like to thoroughly investigate the role of the Lorentz contraction of eigen volumes of hadrons to essentially improve the previous analysis [24, 25, 29] and to study the influence of the hadronic surface tension on the fit of the freeze-out parameters. As we argue the latter may provide us with new information about the critical temperature value of the QCD phase diagram. Such a comprehensive analysis of the different features of the thermal model and the experimental data will also allow us to elucidate the correct criterion of the chemical freeze-out which is a very hot topic nowadays. Furthermore, we perform the simultaneous fit of hadron multiplicities and the  $K^+/\pi^+$  ratio for all available energies of collisions and, hence, for the first time obtain the high quality fit of the Strangeness Horn, i.e. the peak in the  $K^+/\pi^+$  ratio.

The work is organized as follows. The basic features of the thermal model are outlined in the next section. In Section 3 we discuss the important problems related to the conservation laws and propose their solutions. The discussion of the existing chemical freeze-out criteria and formulation of a new criterion along with a novel effect of the adiabatic chemical hadron production is given in

Section 4, while Section 5 is devoted to the model reformulation for the multi-component hadron gas mixture. In Section 6 we investigate the values of the hard-core radii and study the effect of the Lorentz contraction of hard-core spheres. Section 7 is devoted to the analysis of the hadronic surface tension, while in Section 8 we describe the Strangeness Horn. Section 9 contains our conclusions.

## 2. Model formulation

In order to study the role of conservation laws in a form suggested in [2] and employed in their subsequent publications it is, first of all, necessary to reproduce the results obtained in that work. For this purpose let us consider the Boltzmann gas consisting of  $s$  sorts of hadrons having the temperature  $T$  and the volume  $V$ . Each  $i$ -th sort is characterized by its own mass  $m_i$  and chemical potential  $\mu_i$ . Suppose that the number of particles of  $i$ -th sort is  $N_i$ . Then its canonical partition function is

$$Z_{can}(T, V, N_1, \dots, N_s) = \prod_{i=1}^s \left[ \frac{g_i V}{(2\pi)^3} \int \exp\left(-\frac{\sqrt{k^2 + m_i^2}}{T}\right) d^3 k \right]^{N_i}. \quad (1)$$

Here  $g_i = 2S + 1$  is the degeneracy factor of  $i$ -th hadron sort,  $k$  is the particle momentum. The corresponding grand canonical partition function reads as

$$Z_{gr.can.} = \sum_{N_1=0}^{\infty} \dots \sum_{N_h=0}^{\infty} \exp\left[\frac{\mu_1 N_1 + \dots + \mu_s N_s}{T}\right] \times Z_{can}(T, N_1, \dots, N_s). \quad (2)$$

From (2) one gets the number of particles of each sort:

$$N_i = V \phi_i(T, m_i, g_i) \exp\left[\frac{\mu_i}{T}\right] \equiv \frac{g_i V}{(2\pi)^3} \int \exp\left(\frac{\mu_i - \sqrt{k^2 + m_i^2}}{T}\right) d^3 k. \quad (3)$$

Following the commonly accepted approach, we consider the conservation of baryon charge  $B$ , strangeness  $S$  and isospin projection  $I_3$  on average:

$$\sum_{i=1}^N n_i S_i = S_{init} = 0, \quad (4)$$

$$\sum_{i=1}^N n_i B_i = B_{init}/V = 200/V, \quad (5)$$

$$\sum_{i=1}^N n_i I_{3i} = I_{3init}/V = -20/V. \quad (6)$$

These conservation laws define the value of the total chemical potential for the hadron of sort  $i$  as  $\mu_i = B_i \cdot \mu_b + S_i \cdot \mu_s + I_{3i} \cdot \mu_{I_3}$ , where the quantities  $B_i$ ,  $S_i$  and  $I_{3i}$  denote, respectively, the baryonic, strange and isospin projection of such a hadron, while the corresponding chemical potentials are denoted as  $\mu_b$ ,  $\mu_s$  and  $\mu_{I_3}$ .

The interaction of hadrons and resonances is usually accounted for by the hard-core repulsion of the Van der Waals type [5] as

$$p = p_{id.gas} \cdot \exp\left(-\frac{p \cdot b}{T}\right), \quad n_i = \frac{n_i^{id} \exp\left(-\frac{pb}{T}\right)}{1 + \frac{pb}{T}}, \quad (7)$$

where the pressure  $p_{id.gas}$  and the  $i$ -th charge density  $n_i^{id}$  of an ideal gas is modified due to hard-core repulsion. Here  $b = \frac{2\pi}{3}(2R)^3$  is the excluded volume for the hard-core radius  $R$ , which in actual calculations was taken to be  $R = 0.3$  fm for all hadrons. The usual Van der Waals correction affects the particle densities, but has no effect on particle ratios [5]. While its effect on the charge and particle densities may be strong, for the freeze-out densities obtained at and above the highest SPS energy  $\sqrt{S_{NN}} = 17.6$  GeV the excluded volume correction leads to a reduction of the densities by about of 50 percent.

The resonance decays are usually accounted for in the following way: the final multiplicity of hadron  $X$  consists of the thermal contribution  $N_X^{th}$  and the decay ones:

$$N_X^{fin} = N_X^{th} + N^{decay} = N_X^{th} + \sum_Y N_Y^{th} Br(Y \rightarrow X), \quad (8)$$

where  $Br(Y \rightarrow X)$  is the decay branching of the  $Y$ -th hadron into the hadron  $X$ . The masses, the widths and the decay branchings were taken from the particle tables used by the thermodynamic code THERMUS [7].

The width  $\Gamma$  of the resonance of mean mass  $m$  is accounted for by replacing the Boltzmann distribution function in the particle pressure by its average over the Breit-Wigner mass distribution as

$$\int \exp\left(-\frac{\sqrt{k^2 + m^2}}{T}\right) d^3 k \rightarrow \frac{\int_{M_0}^{\infty} \frac{dx_i}{(x_i - m)^2 + \Gamma^2/4} \int \exp\left(-\frac{\sqrt{k^2 + x_i^2}}{T}\right) d^3 k}{\int_{M_0}^{\infty} \frac{dx_i}{(x_i - m)^2 + \Gamma^2/4}}, \quad (9)$$

where  $M_0$  is the dominant decay channel mass.

## 3. Role of conservation laws

Using the thermal model formulated in previous section we fitted the hadron yield ratios in the energy range

from AGS to RHIC, i.e. for  $\sqrt{S_{NN}} = 2.7 \div 200$  GeV. We used the  $\chi^2$  minimization for all the ratios available for this energy range as the fit criterion. The present consideration is very similar to that one used in [2]. The main sources of difference are listed below.

- **The Boltzmann statistics** is used here instead of the quantum statistics employed in [2]. This allows us to essentially fasten the simulations since the momentum integration can be done only once for each hadron species. We checked that for the freeze-out temperatures  $T \geq 50$  MeV obtained here the difference of the results due to the Boltzmann statistics is almost negligible.
- **The charm conservation** is not accounted for by the present model, since it is important only for the charmed particles multiplicities description which is not considered here.
- **The particle table** used here is slightly different from that one of [2], but this does not lead to a big difference in results. Although, in contrast to [2], we do not fit the mass and the width of  $\sigma(600)$  meson.
- **Inclusion of the resonance width** is done in this work for all values of colliding energy  $\sqrt{S_{NN}}$ , while in [2] the width was accounted only for the AGS energy range.

As it is seen from Fig. 1 the experimental hadron yield ratios are reproduced very well within the present model. The dependence of the chemical freeze-out fitting parameters on  $\sqrt{S_{NN}}$  is given in Fig. 2. In Fig. 2 we show only the statistical errors for the obtained fit, while for the parameters of work [2] the shown errors account for the systematic and the statistical ones. As one can see from Fig. 2 the discrepancy between the results of the present model and that one of [2] is within the error bars.

Similarly to [2] we found that both the chemical freeze-out temperature  $T$  and baryonic chemical potential  $\mu_b$  are almost independent of the initial value of the baryon charge  $B_{init}$  and the initial value of the isospin projection  $I_{3_{init}}$ . However, we found that the freeze-out volume  $V$  which stands on the right part side of conservation laws (5) and (6) is very sensitive to them. The obtained chemical freeze-out volume dependence on  $\sqrt{S_{NN}}$  for  $B_{init} = 200$  and  $I_{3_{init}} = -20$  is shown in Fig. 3.

From the larger symbols in Fig. 3 one can clearly see that for the center of mass collision energies  $\sqrt{S_{NN}} =$

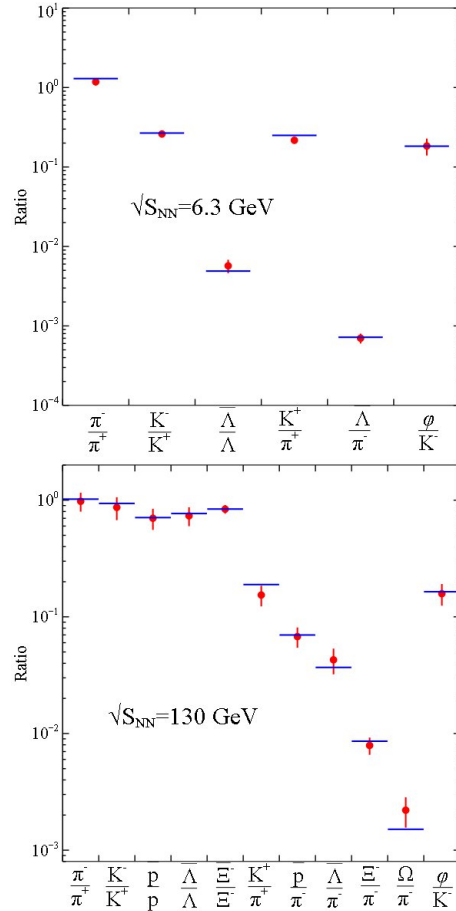


Fig. 1. The examples of the particle yield ratios description. The dots denotes the experimental values, while the lines show the result of fit. Upper panel:  $\sqrt{S_{NN}} = 6.3$  GeV,  $T=139$  MeV,  $\mu_b = 503$  MeV, the mean square deviation per degree of freedom is  $\chi^2/NDF = 4.8/4$ . Lower panel:  $\sqrt{S_{NN}} = 130$  GeV,  $T=169$  MeV,  $\mu_b = 31$  MeV,  $\chi^2/NDF = 3.4/9$ .

$2.7 - 4.3$  and  $\sqrt{S_{NN}} = 12 - 200$  GeV the found chemical freeze-out volume is so large that it exceeds the volume of kinetic freeze-out [9]. Here we found that unlike the hadron yield ratios, the chemical freeze-out volume is very sensitive both to the excluded volume correction and to the values of parameters  $B_{init}$  and  $I_{3_{init}}$ . From Eq. (5) one can deduce that the larger value of the excluded volume  $b$  corresponds to the larger value of the chemical freeze-out volume  $V$  since larger  $b$  value one obtains the smaller particle concentrations  $n_i$  and, consequently, the larger volume  $V = B_{init} / \sum n_i B_i$ . Therefore, the minimal chemical freeze-out volume corresponds to an ideal gas, i.e. for  $b = 0$ . This minimal chemical freeze-out volume is also shown in Fig. 3. Despite the absence of the excluded volume correction,

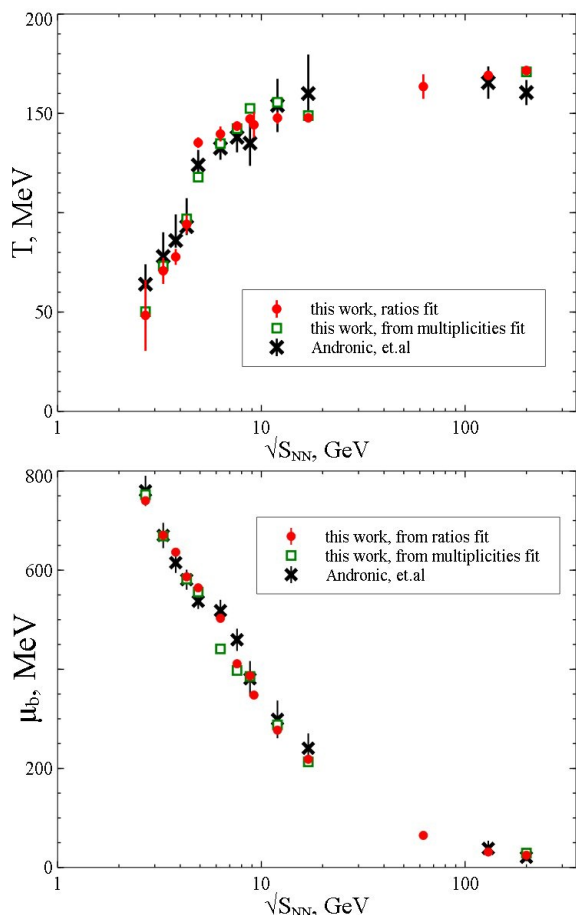


Fig. 2. Dependence of thermal model fitting parameters on the center of mass collision energy  $\sqrt{S_{NN}}$ . Upper panel: the chemical freeze-out temperature  $T$  vs.  $\sqrt{S_{NN}}$ . Lower panel: the chemical freeze-out baryonic chemical potential  $\mu_b$  vs.  $\sqrt{S_{NN}}$ . The results obtained from the fit of hadron yield ratios (circles) with the conservation laws and from the fit of hadron multiplicities (open squares) are compared with that ones obtained in [2] (crosses).

chemical freeze-out volume for an ideal gas remains huge. Hence, we conclude that the initial values in conservation laws, namely  $B_{init}$  and  $I_{3_{init}}$  are of crucial importance for an extraction of chemical freeze-out volume.

From the comparison of the hadron multiplicity  $N = n \cdot V$  obtained by the thermal model and its experimental value  $dN/dy|_{y=0}$  measured at zero rapidity, one can conclude whether the thermal model provides a reliable description of hadron multiplicities. Such a comparison for  $\pi^+$  and  $K^+$  mesons is shown in Fig. 4. Since the hadron yield ratios shown in Fig. 1 are described well by the thermal model, then one would expect that, if the multiplicity of a single hadron type is in a good agreement with the experiment data, then the multiplicities

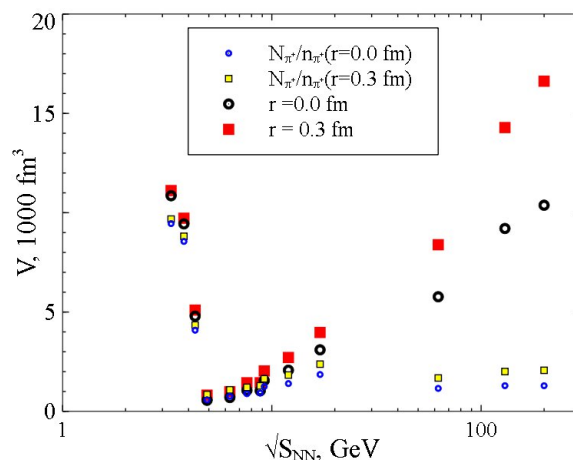


Fig. 3. The chemical freeze-out volume vs.  $\sqrt{S_{NN}}$  for the ideal hadron gas and the hadron gas with the hard-core radii 0.3 fm. The smaller symbols correspond to the fit of hadron yield ratios with all the conservation laws (4)-(6) accounted for, while the larger symbols are obtained by the fit of hadron multiplicities ignoring Eq. (5) (see text for details).

of all other sorts of hadrons should be well described too. However, from Fig. 4 one can see that at  $\sqrt{S_{NN}} \geq 10$  GeV the experimental values of multiplicities are much smaller than the theoretical ones. At lower  $\sqrt{S_{NN}}$  there is no such a problem, despite the big chemical freeze-out volume  $V$ . Our conclusion is that for higher energies the value of parameters  $B_{init}$  and  $|I_{3_{init}}|$  should be taken smaller than for lower energies. In particular, according to Fig. 4 at  $\sqrt{S_{NN}} = 200$  GeV the value of  $B_{init}$  and  $|I_{3_{init}}|$  should be about 10 times smaller than at ones for the low collision energies.

A different way to describe the hadron multiplicities was used in [2]. The chemical freeze-out volume  $V$  was treated there as a free parameter. Let's show that such a treatment leads to mathematical ambiguity. Consider the conservation laws (4)-(6) together with the following expression for system pressure

$$p = p^{id}(T, \mu_b, \mu_s, \mu_{I_3}) \cdot \exp\left(-\frac{pb}{T}\right). \quad (10)$$

Such a system of equations has six unknowns, i.e.  $T$ ,  $\mu_b$ ,  $\mu_s$ ,  $\mu_{I_3}$ ,  $V$ ,  $p$ , and four equations. Hence, two unknowns should be treated as free fitting parameters. If, however, one treats three unknowns as free parameters, then one of the equations may be not satisfied in general. More specifically, if  $T$ ,  $\mu_b$  and  $V$  are the free fitting parameters, then the baryon charge conservation equation (5) may be broken down. To demonstrate this explicitly we have considered the thermal model fit with three

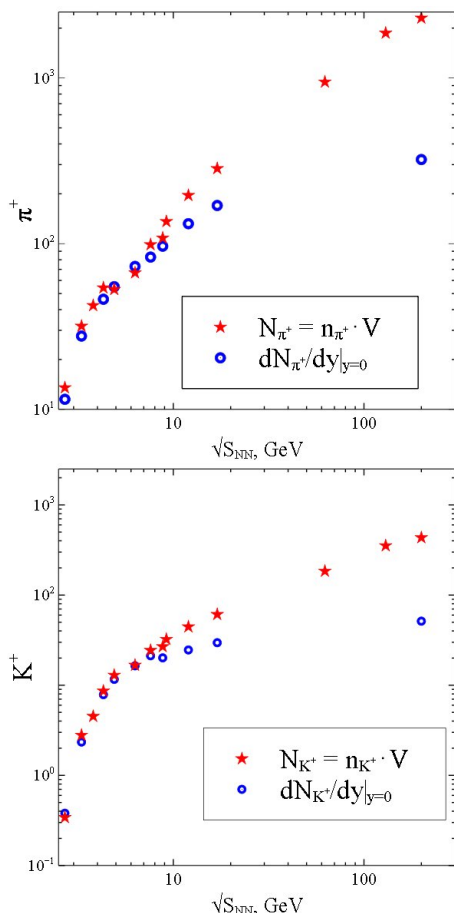


Fig. 4. Upper panel:  $\pi^+$  multiplicity at chemical freeze-out vs.  $\sqrt{S_{NN}}$ . Lower panel:  $K^+$  multiplicity at chemical freeze-out vs.  $\sqrt{S_{NN}}$ . The circles correspond to the experimental data, whereas the stars are found from particle densities as  $N = n \cdot V$

free parameters -  $T$ ,  $\mu_b$  and  $V$  and ignored the baryon charge conservation equation (5), while the isospin projection conservation law (6) was used to find the chemical potential  $\mu_{I_3}$ . After fitting the experimental hadron multiplicities  $dN/dy|_{y=0}$  (not their ratios!) for the same energy range as before, we found the resulting baryonic charge as  $S_b = V \cdot \sum_{i=1}^N n_i B_i$  summing up the densities  $n_i$  of all baryons and anti-baryons multiplied by their baryonic charge  $B_i$ . Clearly, if Eq. (5) is satisfied, then this sum  $S_b$  should match the value of  $B_{init} = 200$ . Fig. 5, however, demonstrates that Eq. (5) cannot be satisfied. Although the chemical freeze-out temperature and baryonic chemical potential obtained by the fitting of the hadron multiplicities do not differ essentially from that ones found by the fit of hadron yield ratios (see open squares in Fig. 2), the freeze-out volumes obtained from the multiplicity fit are essentially smaller (see smaller

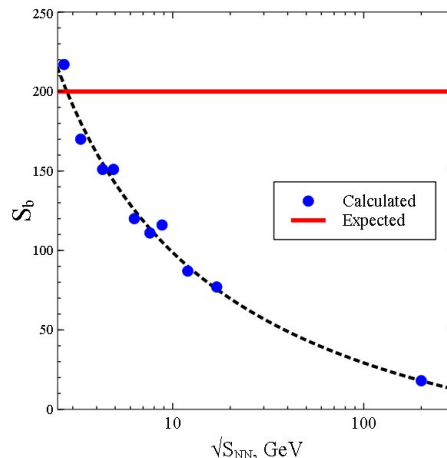


Fig. 5. The obtained baryonic charge  $S_b = V \cdot \sum_{i=1}^N n_i B_i$  (dots) vs.  $\sqrt{S_{NN}}$ . The dots are calculated from the baryon charge conservation, whereas the line corresponds to the expected value  $B_{init} = 200$ .

symbols in Fig. 3) and more physically adequate for  $\sqrt{S_{NN}} \geq 5$  GeV than that ones found from the fit of hadron yield ratios.

Additionally, here we found that the values of  $B_{init}$  and  $I_{3_{init}}$  should strongly depend on collision energy: at  $\sqrt{S_{NN}} = 200$  GeV they are about ten times smaller than at the AGS energies. The hadron yield ratios are not sensitive to the values of  $B_{init}$  and  $I_{3_{init}}$ , and hence the baryon charge and  $I_3$  conservation can be neglected for the description of hadron yield ratios. If, however, one supposes that  $B_{init} = const > 0$  and  $I_{3_{init}} = const > 0$ , then the description of hadron multiplicities completely fails. Evidently, one can describe the hadron multiplicities by introducing  $\sqrt{S_{NN}}$  dependence of  $B_{init}$  and  $I_{3_{init}}$  values, if such dependences are known. Since such dependences are unknown, then one has to ignore the baryon charge (5) and isospin projection (6) conservation laws, and to fit the parameters  $T$ ,  $\mu_b$ ,  $\mu_{I_3}$  and  $V$  to describe the hadron multiplicities or to fit the parameters  $T$ ,  $\mu_b$ ,  $\mu_{I_3}$  in order to get the description of hadron yield ratios. Note, however, that the strangeness conservation laws (4) does not create such problems and, hence, it should be always obeyed.

#### 4. Chemical freeze-out criteria and adiabatic chemical hadron production

The thermal model discussed above allows us to clarify the long standing question on the physically appropriate chemical freeze-out criterion which is widely discussed [22, 23]. The most popular chemical freeze-out crite-

ria are (I) the constant value of the mean energy per hadron,  $\langle E \rangle / \langle N \rangle \simeq 1.08$  GeV, (II) the constant value of the entropy density to the cube of the temperature,  $s/T^3 \simeq 7$ , and (III) the constant value of a total baryon and antibaryon density  $n_B + n_{\bar{B}} \simeq 0.12$  fm $^{-3}$ . The criterion (I) is believed to be more robust, while the criteria (II) and (III) show strong dependence on the hard-core radius value [23]. We have performed the analysis and found the criteria (II) and (III) are not obeyed at all, while the criterion (I) validity depends essentially on the thermal model parameterization. The validity of these statements for the criteria (I) and (II) are, respectively, demonstrated in the middle and the upper panels of Fig. 6. Moreover, the thermal model results that we extracted from [2] are very similar to our ones, despite several differences in the parameterization of these two models.

Our detailed analysis shows that there exists a much more robust chemical freeze-out criterion than all previously discussed ones. This novel criterion corresponds to the constant value of the entropy per number of particles which in terms of the entropy density  $s$  and hadron number density  $\rho_{part}$  can be expressed as

$$\frac{s}{\rho_{part}} \simeq 7.18. \quad (11)$$

The lower panel of Fig. 6 shows that for two different parameterizations of the thermal model the ratio  $\frac{s}{\rho_{part}}$  stands between 6.6 and 7.6, i.e. the deviates within  $\pm 8\%$  only, while the values of the center of mass energy of collision change for two orders of magnitude! Such a behavior of the  $\frac{s}{\rho_{part}}$  quantity evidences for the **adiabatic chemical hadron production** in heavy ion collisions.

## 5. Multi-component gas and hard-core radii

Although it is clear that the hadron radii can serve as the parameters of the thermal model, they, however, are rarely treated as the free parameters. The common approach is to fix one radius for all hadrons. The value of this radius was discussed [11] and it ranges from 0.2 fm to 0.8 fm [12]. However, the value  $r=0.3$  fm that was taken from nucleon-nucleon scattering [10] seems to be an established value. To investigate the role of the hard-core radii we introduce the different radii for mesons and for baryons  $R_m$  and  $R_b$ , respectively. Also to study an influence of the Lorentz contraction of hard-core radii on the chemical freeze-out parameters  $T$ ,  $\mu_b$  and on the hadron yield particle ratios we need the hadron gas model which

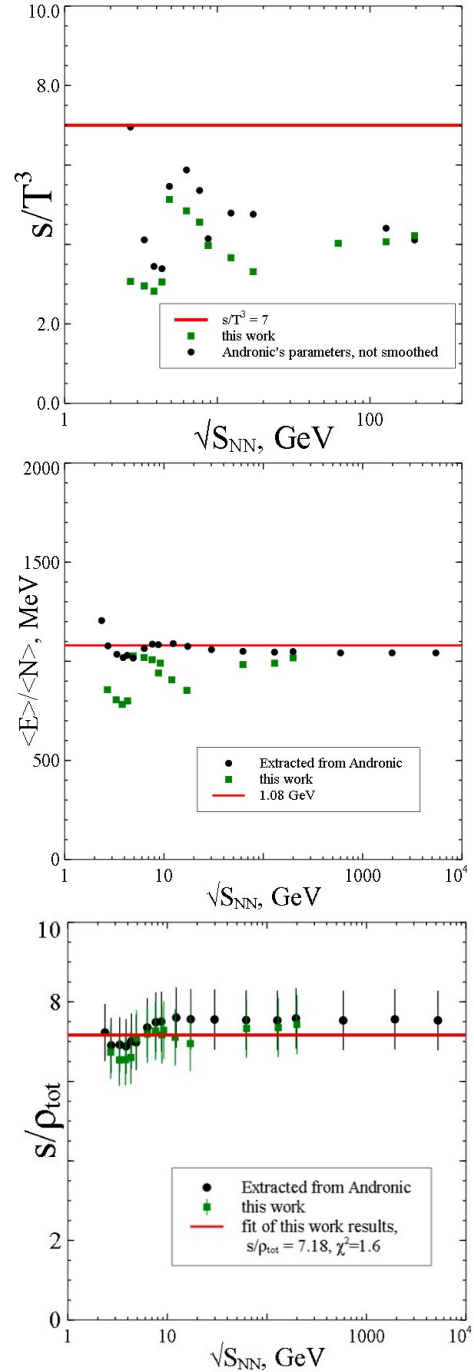


Fig. 6. Different chemical freeze-out criteria. Upper panel: ratio of the entropy density to the cube of temperature  $s/T^3$  at chemical freeze-out vs.  $\sqrt{S_{NN}}$ . Middle panel: energy per particle  $\langle E \rangle / \langle N \rangle$  at chemical chemical freeze-out vs.  $\sqrt{S_{NN}}$ . Lower panel: the novel criterion of chemical freeze-out, entropy per particle at chemical freeze-out  $s/\rho \simeq 7.18$ . The shown errors are combined the statistical and systematic errors. The results of present work (squares) are very similar with that ones extracted from [2].

accounts for different values of their eigen volumes. For this purpose we use an approach developed in [24, 25, 29]. Below we give the necessary theoretical apparatus to study the multi-component hadron gas mixture, whereas the results of the global fit for the cases with and without Lorentz contraction are given in the subsequent section.

Consider again the Boltzmann gas of  $s$  hadron species in a volume  $V$  at a temperature  $T$ . Let  $N_i$  be a quantity of the  $i$ -th sort of hadrons

$$N = \begin{pmatrix} N_1 \\ N_2 \\ \dots \\ N_s \end{pmatrix}. \quad (12)$$

The total number of particles is  $M = \sum_{i=1}^s N_i$ . It is assumed that for every two sorts of hadrons  $i$  and  $j$  there is the excluded volume  $b_{ij}$ . Then one can introduce the excluded volume matrix  $B = (b_{ij})$ . Naturally, it is supposed that the matrix  $B$  is symmetric, i.e.  $b_{ij} = b_{ji}$ .

The canonical partition function can be obtained by adding the particles of some eigen volume one-by-one and taking in account all the corresponding excluded volumes of the previously added particles. Such an approximation was suggested in [25] and it gives the following expression for the canonical partition of the Van der Waals hadron gas mixture

$$Z_{VdW}(T, V, N_i) = \left[ \prod_{i=1}^s \frac{\phi_i^{N_i}}{N_i!} \right] \times \left[ V - \frac{N^T B N}{M} \right]^M \quad (13)$$

where the thermal particle density  $\phi_i(T, m, g)$  is defined in (3), and  $N^T$  is the transposed matrix to that one given by (12).

In the next step we write the grand canonical partition function (GCPF) as

$$\mathcal{Z} = \sum_{N_1=1}^{\infty} \sum_{N_2=1}^{\infty} \dots \sum_{N_s=1}^{\infty} \left( \prod_{i=1}^s \exp \left[ \frac{\mu_i N_i}{T} \right] \right) \times Z_{VdW}. \quad (14)$$

It is well known [31] that in the thermodynamic limit the GCPF can be replaced by the maximal term of the multiple sum in  $\mathcal{Z}$  (the maximum term method). Suppose that the array  $N^*$  gives the maximal term of  $\mathcal{Z}$ . Then the system pressure is given by

$$p/T = \lim_{V \rightarrow \infty} \frac{\mathcal{Z}}{V} = \lim_{V \rightarrow \infty} \frac{1}{V} \ln \left[ \prod_{i=1}^s \frac{A_i^{N_i^*}}{N_i^{*!}} \times \left( V - \frac{(N^*)^T B N^*}{M^*} \right)^{M^*} \right], \quad (15)$$

where  $A_i = \phi_i \exp \left[ \frac{\mu_i}{T} \right]$ . Let us find  $N^*$  from the maximum conditions ( $i = 1..s$ ):

$$\frac{\partial}{\partial N_i^*} \left[ \ln \left[ \prod_{i=1}^s \frac{A_i^{N_i^*}}{N_i^{*!}} \left( V - \frac{(N^*)^T B N^*}{M^*} \right)^{M^*} \right] \right] = 0. \quad (16)$$

Performing the differentiations, one gets

$$\xi_i = A_i \exp \left( - \sum_{j=1}^s 2\xi_j b_{ij} + \frac{\xi^T B \xi}{\sum_{j=1}^s \xi_j} \right), \quad (17)$$

with  $\xi_i = \frac{N_i}{V - \frac{N^T B N}{M}}$  and

$$\xi = \begin{pmatrix} \xi_1 \\ \xi_2 \\ \dots \\ \xi_s \end{pmatrix}. \quad (18)$$

Using (17) one can express the hadron densities  $n_i = \frac{N_i^*}{V}$  and the system pressure  $p$  as

$$n_i = \frac{\xi_i}{1 + \frac{\xi^T B \xi}{\sum_{j=1}^s \xi_j}}, \quad p = T \sum_{i=1}^s \xi_i \quad (19)$$

The solution of the system of equations (17)–(19) defines the hadron densities for the multi-component gas.

In a special case when all the elements of the excluded volumes matrix are equal  $b_{ij} = v_0$  Eqs. (17)–(19) give

$$\begin{cases} \xi_i = A_i \exp(-p v_0/T), \\ n_i = \frac{\xi_i}{1 + p v_0/T}, \\ p/T = \left( \sum_{i=1}^s A_i \right) \cdot \exp(-p v_0/T). \end{cases} \quad (20)$$

In this case the ratios of two particle densities from (20) match that ones of the mixture of the corresponding ideal gases for an arbitrary value of  $v_0$ , while the particle densities themselves may essentially differ from the particle densities of the ideal gas.

## 6. Results for hard-core radii with the Lorentz contraction

In this subsection it is assumed that all baryons have the same hard-core radii  $R_b$  and all mesons have the same hard-core radii  $R_m$ . Then performing the global fit we would like, first, to find the pair of radii  $(R_m, R_b)$  that provides the best fit, and, second, we would like to study the influence of Lorentz contraction of the chemical freeze-out parameters.

To simplify the numerics let us define that two hadrons belong to the same type, if their excluded volumes are



equal. The number of equations in the system (17) is equal to the number of particle types. Hence, the case with the Lorentz contraction included is more complicated, because instead of two sets of particles one should treat each hadron type as a new kind of particles. In order to avoid the large number of equations in system (17), the particles heavier than 900 MeV are considered non-relativistically, i.e. they all belong to two sorts: either to the baryons with the hard-core radius  $R_b$  or to heavy mesons with hard-core radius  $R_m$ . For two particles  $i$  and  $j$ , both heavier than 900 MeV, the element of excluded volume matrix  $b_{i,j}$  is  $\frac{2\pi}{3}(R_i + R_j)^3$ . For other cases the second virial coefficients  $b_{i,j}$  are calculated using Eqs. (3) and (4) of [29] by the direct translation of one ellipsoid around the other with the subsequent averaging of the obtained excluded volume over the ellipsoid positions.

The fit procedure is the same as described in the preceding subsection: we fit the hadron yield ratios by  $T$ ,  $\mu_b$  and  $V$ , respect the isospin projection conservation law (6) to find the value of  $\mu_{I_3}$ , but ignore the baryonic charge conservation law (5). This our effort to study the role of the Lorentz contraction is inspired by the fact that the conventional thermal model has problems with the light mesons description. Thus, to describe the pion multiplicity and the ratios containing the pions it was proposed to introduce  $R_\pi$  which is smaller than all the other hadron radii [5, 30]. Another example of difficulties with the light mesons is a "Strangeness Horn", i.e. the peak in the  $K^+/\pi^+$  ratio. Its description was finally improved by fitting the  $\sigma(600)$  meson mass and width [3], but the obtained description is far from being very good.

Let us see whether the Lorentz contraction might resolve these problems. At a given temperature the eigen volume of the lighter particles decrease more than that one of the heavier ones. Consequently, the excluded volume of lighter particles gets smaller compared to the excluded volume of heavier ones [24, 25, 29]. Such a behavior of the Lorentz contracted excluded volume provides us with the natural explanation of the fact that pion hard-core radius  $R_\pi$  is smaller than other hard-core radii. On the other hand, this might improve the Strangeness Horn description. It was also shown [29] that the Lorentz contraction removes the causality paradox from the thermal model, i.e. at high densities the speed of sound does not exceed the speed of light. Therefore, it is necessary to incorporate the Lorentz contraction into conventional thermal model and study its effect on the hadron multiplicity description. In order to make the numerical evaluation of the relativistic excluded volumes faster we

heuristically derived an approximative formula for such volumes which allows one to reduce the six dimensional integration over the pair of three-vectors of particle momenta to the three dimensional integral. The derivation of such a formula and its verification are given in the Appendix.

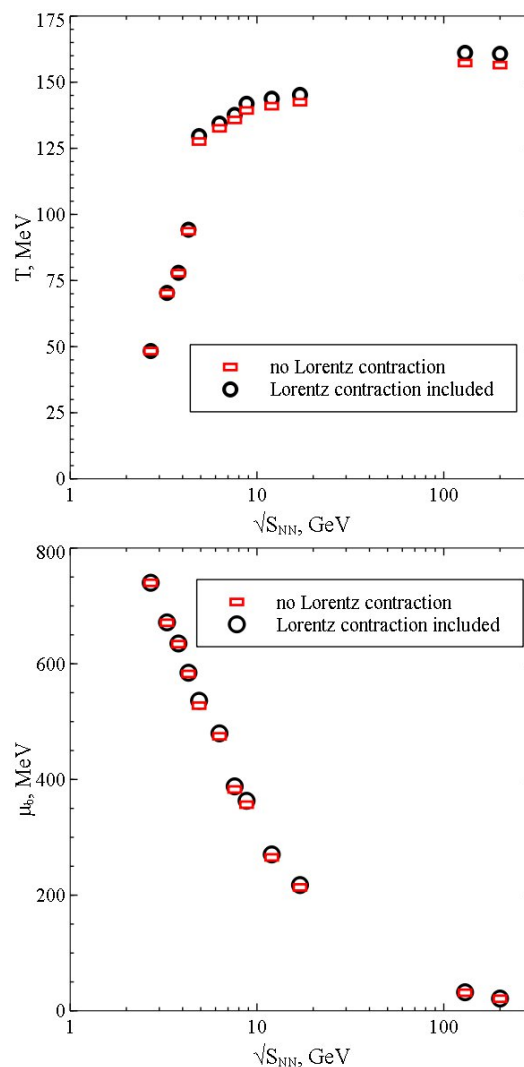


Fig. 7. The chemical freeze-out parameters obtained from the fit with (circles) and without (rectangles) the Lorentz contraction. Upper panel: the chemical freeze-out temperature  $T$  vs.  $\sqrt{S_{NN}}$ . Lower panel: the chemical freeze-out baryonic chemical potential  $\mu_b$  vs.  $\sqrt{S_{NN}}$ .

To compare the models with and without the Lorentz contraction, we have chosen hard-core radii  $R_m=0.45$  fm,  $R_b = 0.3$  fm and have found the new best-fit  $T$  and  $\mu_b$  values for the case with Lorentz contraction, see Fig. 7. From this figure one can conclude that the baryo-

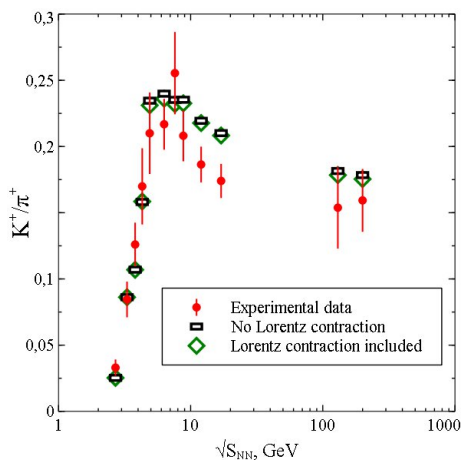


Fig. 8. Strangeness Horn description improvement for the model with the Lorentz contraction included and without it.

chemical potential is almost unaffected by the Lorentz contraction, while the temperature is slightly higher for the case with the Lorentz contraction. It is also interesting to check, whether the inclusion of the Lorentz contraction improves the Strangeness Horn description. From Fig. 8 we conclude that there is a small improvement, which is not sufficient to qualitatively improve the Strangeness Horn description.

The important result, however, is that the Lorentz contraction inclusion provides us with the better fit quality for any pair of radii ( $R_m, R_b$ ). From Fig. 9 one can see the difference between the  $\chi^2/NDF$  values found without the Lorentz contraction and with it. Obviously, when both radii are small, then the correction due to the Lorentz contraction is small too. At  $(R_b, R_m) = (0.3, 0.4)$  fm  $\Delta\chi^2/NDF \approx 0.1$ , while  $\chi^2/NDF$  itself is 1.48.

The simplest way to obtain the best fit radii is to perform a global fit, including the radii into the fitting procedure. However, in the  $(R_m, R_b)$  plane there exist the domains, where  $\chi^2$  stays almost unchanged. For example, in the case without the Lorentz contraction  $\chi^2$  is the same along the line  $R_b = R_m$ , which follows directly from (20). This makes the straightforward global fit rather difficult. Therefore, we perform the fit procedure of particle ratios in central nucleus-nucleus collisions at  $\sqrt{S_{NN}} = 2.7, 3.3, 3.8, 4.3, 4.9, 6.3, 7.6, 8.8, 12, 17, 130, 200$  GeV for each pair of the radii  $(R_m, R_b)$  and find the domains, where  $\chi^2$  differs from its minimal value less than 10%. The results are shown in Fig. 10.

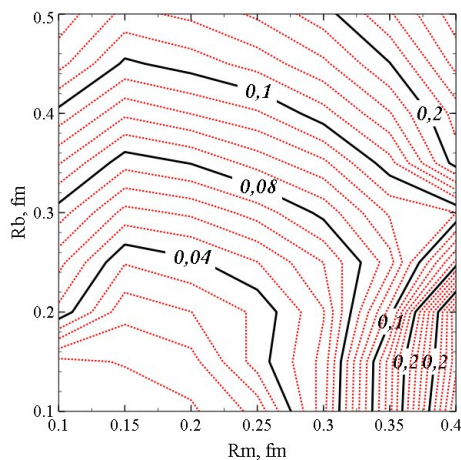


Fig. 9. Difference of  $\chi^2/NDF$  between the model without the Lorentz contraction and the model with it for different values of meson and baryon hard-core radii.

## 7. Determination of hadronic surface tension

Recently the extremely important role of the surface tension of quark gluon bags was realized within the exactly solvable models for the deconfinement phase transition with the tricritical [32,33] and the critical [34] endpoints. It was shown [32–34] that the (tri)critical endpoint appears due to vanishing surface tension coefficient, while at low baryonic densities the deconfinement phase transition degenerates into a cross-over just due to the negative values of surface tension coefficient. The existence of negative values of the surface tension coefficient at the cross-over temperature for demonstrated analytically within the model of color confining tube [35]. Using this model it was possible to predict the value of (tri)critical temperature of QCD phase diagram  $T_{cep} = 152.9 \pm 4.5$  MeV [36] using the plausible assumption on the temperature dependence of the surface tension coefficient  $\sigma(T) = a^2 \left(1 - \frac{T}{T_{cep}}\right)$  [37] which is typical for ordinary liquids.

Since the lattice QCD is not reliable at the non-zero values of the baryonic chemical potential it would be interesting to study the surface tension for hadrons at the chemical freeze-out. The surface free energy can be written as  $F_{surf} = \sigma(T)S$ , where the hadron surface  $S$  is given by its hard-core radius  $R$  as  $S = 4\pi R^2$ . Note that such a parameterization of the surface free energy is typical for the multi-component gas mixtures [32–34, 38]. Inclusion of the surface free energy into the thermal model is equivalent to adding the term  $\sigma(T)S$  to the total chemical potential. If  $S$  is the same for all hadrons, such

Collision energies set, $\sqrt{S_{NN}}$	$\chi^2/NDF$ without surface tension	$\chi^2/NDF$ with surface tension	$\sigma_0$ , MeV fm $^{-2}$	$T_0$ , MeV
2.7 - 7.6	25.8135/33 = 0.782	25.8043/31 = 0.832	$0.91 \cdot 10^{-2}$	61
2.7 - 200	103.096/82 = 1.2573	103.036/80 = 1.288	$-1.37 \cdot 10^{-2}$	57
2.7 - 62.4 (no 130 and 200)	85.51/65 = 1.3156	85.268/63 = 1.3534	$-3.21 \cdot 10^{-2}$	62
12, 17, 62.4, 130, 200	62.5452/37 = 1.69	62.1454/35 = 1.776	0.654	147

**Table 1.** Results of the global fit, including the extracted surface tension parameters.

a surface tension correction does not affect the hadron yield ratios. Therefore, we have taken  $R_m = 0.45$  fm,  $R_b = 0.3$  fm, to have the noticeable radii difference. In the actual simulations the surface tension coefficient  $\sigma(T)$  was parameterized as

$$\sigma(T) = \sigma_0 \left( 1 - \frac{T}{T_0} \right). \quad (21)$$

Here  $\sigma_0$  and  $T_0 > 0$  are the free parameters to be found from a global fit. Note that for  $T \leq T_0$  such a temperature dependence coincides with the famous Fisher droplet model parameterization [37], whereas for  $T > T_0$  it is in line with the recent findings [32–36]. We have performed several global fits with the parameterization (21), using different data sets. The results are listed in the Table 1.

From this table one can conclude that the inclusion of the surface tension in the form (21) does not improve the fit quality, however, since in all cases the value of  $\chi^2/NDF$  is almost the same as without accounting for the surface tension, it also does not spoil the fit quality. This fact allows us to take the obtained values of parameters  $\sigma_0$  and  $T_0$  rather seriously. It is not surprising, that the value of  $\sigma_0$  is close to zero, otherwise the sizable surface tension of hadrons could be already found. The really surprising fact is that for the center of mass energies  $\sqrt{S_{NN}} \geq 12$  GeV the parameter  $T_0 = 147 \pm 7$  MeV is extremely close to the critical temperature value  $T_{cep} = 152.9 \pm 4.5$  MeV found in [36] more than a year ago using entirely different approach. Of course, the reason of why the global fit that includes the low energy data gives essentially lower value of the parameter  $T_0$  should be understood, and, hence, the investigation of the hadronic surface tension should be continued using both the experimental data on hadron production and the lattice QCD data.

## 8. Multi-component hadron gas and the Strangeness Horn description

The thorough analysis performed above led us to a conclusion that besides the hadron surface tension inclusion the further improvement of the thermal model can

be achieved, if we consider the pion and kaon hard-core radii, as an independent fitting parameters. On the one hand this would allow us to have two additional fitting parameters, and on the other hand one could include the Strangeness Horn data into the fitting procedure. Note that up to now the quality of the Strangeness Horn description is far from being satisfactory, although very different formulations of the thermal model are used for this purpose [2, 30, 39]. Thus, the most recent compilation of the Strangeness Horn description by the different thermal models can be found in [39].

To improve the Strangeness Horn description can be easily understood from the fact that just the non-monotonic behavior of the  $K^+/\pi^+$  ratio as the function of the center of mass energy of collision is often claimed to be one of a few existing signals of the onset on deconfinement [40–42]. The multi-component hadron gas model developed in [25] is perfectly suited to treat the pion and kaon hard-core radii as independent fitting parameters. The physical idea behind such an approach is that the hadronic hard-core radii are the effective parameters which include the contributions of the repulsion and attraction. Since the parameters of hadron-hadron interaction are, generally speaking, individual for each kind of hadrons, then each kind of hadrons can have its own hard-core radius. Based on this idea we performed a global fit of all hadron multiplicities as described above together with the Strangeness Horn data considering the pion hard-core radius  $R_\pi$  and the kaon hard-core radius  $R_K$  as independent variables together with the chemical freeze-out temperature and baryonic chemical potential, whereas the hard-core radius of all other mesons and the hard-core radius of baryons were fixed, respectively, as  $R_b = 0.3$  fm and  $R_m = 0.5$  fm according to the findings of Section 6.

The results of such a fit are shown in Fig. 11. Comparing Figs. 8 and 11 one can see the dramatic improvement of the  $K^+/\pi^+$  ratio for the collision energies  $\sqrt{S_{NN}}$  above 8 GeV. In fact, the  $K^+/\pi^+$  ratio shown in Fig. 11 deviates from the experimental error bars on for the energy  $\sqrt{S_{NN}} = 3.8$  GeV, while for all other collision energies it does not essentially deviate from the experimental error bars. Thus, the variations of pion and

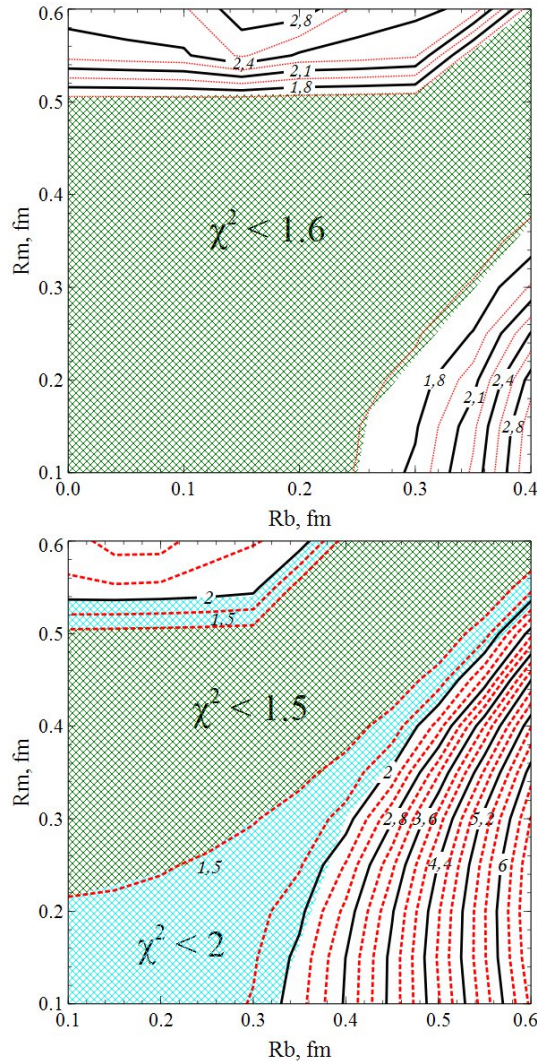


Fig. 10. Upper panel:  $\chi^2/NDF$  for the model without the Lorentz contraction for different values of meson and baryon hard-core radii. Lower panel: same as in the upper panel, but for the model with the Lorentz contraction included.

kaon hard-core radii essentially improve the description of this ratio for all collision energies, but at the same time the quality of the fit of all other hadronic multiplicities does not worsen as it is seen from the resulting value of  $\chi^2/NDF \simeq 1.019$  for the global fit, which, so far, is the best result obtained in the literature.

## 9. Conclusions

In this work we performed a comprehensive analysis of the experimental hadron multiplicities within the thermal model. As in previous studies the considered ther-

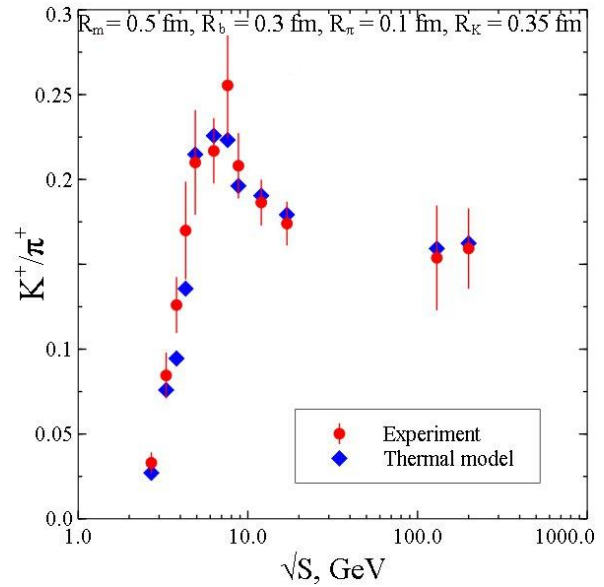


Fig. 11. Strangeness Horn description for the model with pion and kaon hard-core radii to be independent fitting parameters. The resulting quality of the global fit is  $\chi^2/NDF \simeq 1.019$ .

mal model has two hard-core radii ( $R_b$  for baryons and  $R_m$  for mesons) and two new elements: an inclusion of the Lorentz contraction of eigen volumes of hadrons and a treatment of hadronic surface tension. Using this model we studied the role of the imposed conservation laws (5) and (6), and showed that for the adequate description of hadron multiplicities the conservation laws should be modified, whereas for the description of hadron yield ratios the conservation laws are not necessary at all. In addition, we suggested and analyzed the thermal model in which the pion and kaon hard-core radii are independent fitting parameters compared to all other mesons.

Here we also analyzed the usual criteria for the chemical freeze-out and found that none of them is robust. Therefore we suggested a novel criterion of chemical freeze-out, a constant value of entropy per hadron number equals to 7.18. Such a criterion is also supported by the different formulation of thermal model [2] and it evidences for the new physical effect which we called the **adiabatic chemical hadron production**.

The performed analysis allowed us to find the restrictions on the hard-core radii that are imposed by the experimental data. Also we showed that although an inclusion of the Lorentz contraction improves the fit quality for any pair of baryon and meson hard-core radii, but at the same time it has a small effect on the chemical freeze-out parameters and on  $K^+/\pi^+$  ratio.

In addition we phenomenologically introduced the surface tension in thermal model and made several global fits to find its parameters. Although, the surface tension inclusion does not improve the fit quality, for the first time it is found that the temperature of the nil surface tension value depends on the considered interval of the collision energy. Thus, if the low energy data are included into the fit, then the nil surface tension temperature is about  $60 \pm 5$  MeV, while the data for the center of mass energies above 10 GeV lead to an essentially larger value of this temperature value  $T_0 = 147 \pm 7$  MeV. The latter is a very intriguing result since a very close estimate for the nil surface tension temperature was obtained recently within entirely different analysis of the quark gluon bag surface tension [35]. Therefore, it is possible that these two independently obtained results, indeed, evidence that the (tri)critical temperature of the QCD phase diagram is between 140 and 154 MeV.

The most dramatic numerical effect, however, is obtained for the truly multi-component hadron gas model worked out in [25] and employed here for the first time. In this model the hard-core radii of pions and kaons differ from the hard-core radius of all other mesons and they are treated as independent fitting parameters. Such an approach allowed us for the first time to simultaneously fit the hadron multiplicities together with the Strangeness Horn and to get the chemical freeze-out data description of very high quality.

## 10. Appendix: Heuristic derivation of the approximate excluded volume formula for ellipsoids of revolution

In order to fasten the numerical evaluation of the relativistic excluded volumes we would like to obtain an approximate expression which would reduce the dimension of momentum integrations of two particles from six to three. Basically here we employ the heuristic method suggested in [29]. The main difference, however, is that in [29] the ultra-relativistic expression for the excluded volume was derived, while here we would like to get an expression which would be accurate both in the non-relativistic and ultra-relativistic limits.

For this purpose let us consider two relativistic spheres  $S_1$  and  $S_2$ , their  $\gamma$ -factors being  $\gamma_1$  and  $\gamma_2$ , respectively. The hard-core radii in their rest frames are  $R_1$  and  $R_2$ , respectively. Let us fix an angle  $\theta$  between the momenta of two particles which is the standard spherical angle. It is chosen in such a way that the three momentum of  $S_1$  coincides with  $OZ$ -axis (see Figs. 12 and 13 for details). Then the angle  $\theta$  is the azimuthal spherical angle of the

momentum of second particle. Due to the Lorentz contraction the both spheres shrink in the direction of their momenta and one obtains two ellipsoids of revolution. Here we show how to get an approximate formula for the excluded volume for such ellipsoids.

The basic idea is to neglect the complexity of the problem and treat the excluded volume as an ellipsoid, afterwards to symmetrize the obtained expression with respect to interchange  $1 \leftrightarrow 2$  and take the half of the sum of two expressions. Then, the unsymmetrized excluded volume reads:

$$V_{exc} = \frac{4}{3}\pi R_x R_y R_z, \quad (22)$$

where the ellipsoid's radii  $R_x$ ,  $R_y$ ,  $R_z$  are found from geometrical consideration given below.

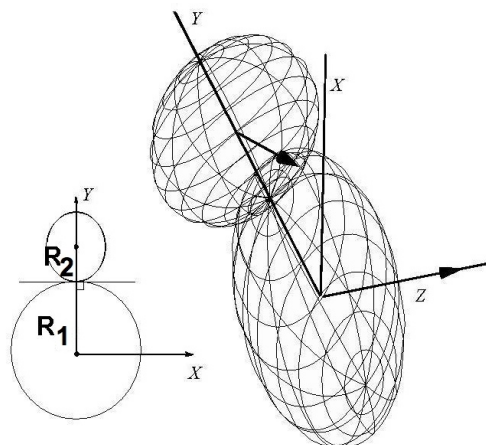


Fig. 12. Explanation on how to obtain the expression for the radius  $R_y$  of the relativistic excluded volume, when the second ellipsoid is translated around the first one in the plane XOY.

From Fig. 12 one can see that

$$R_y = R_1 + R_2. \quad (23)$$

To obtain the radius  $R_x$  one should consider the ellipsoids depicted in Figs. 13–15. The radius  $R_z$  can be found analogously to the radius  $R_x$  from Fig. 16.

Let us show how one can get an expression for the radius  $R_x$ . A convenient projection and the notations are depicted in Figs. 13 and 14. From Fig. 14 one gets

$$R_x = R_1 + \Delta x. \quad (24)$$

Turning the reference frame to the main axes  $x_2$  and  $y_2$  of  $S_2$  (see fig. 15) one easily finds the coordinates

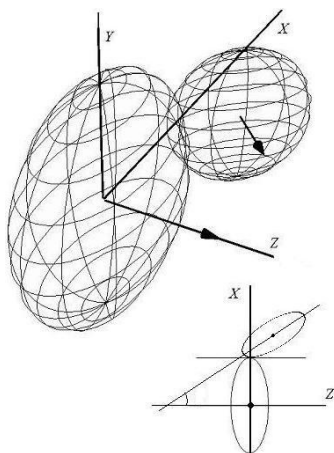


Fig. 13. Explanation on how to obtain the expression for the radius  $R_x$  of the relativistic excluded volume, when the second ellipsoid is translated around the first one in the plane XOZ.

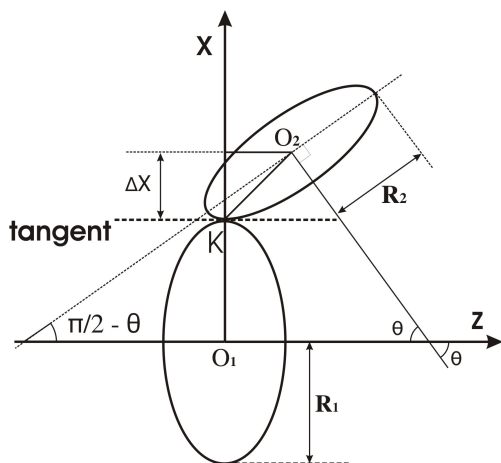


Fig. 14. The detailed projection of the second ellipsoid translation around the first one in the plane XOZ. This is an explanation on how to derive  $R_x$  from Fig. 13.

of touching point  $K(x_0, y_0)$ . The equation of  $S_2$  for the principal axes shown in Fig. 15 reads as:

$$x_2^2 + y_2^2 \gamma_2^2 = R_2^2. \quad (25)$$

The equation for a tangent to an ellipse shown in Fig. 15 is:

$$\frac{dy_2}{dx_2} = -\frac{x_2}{\gamma_2^2 y_2} = \text{tg}(\pi/2 - \theta). \quad (26)$$

Now solving (25) together with (26) one gets the touching point coordinates  $x_0$  and  $y_0$ :

$$x_0 = -\frac{R_2 \gamma_2 \text{ctg} \theta}{\sqrt{1 + \gamma_2^2 \text{ctg}^2 \theta}}, \quad (27)$$

$$y_0 = \frac{R_2}{\gamma_2 \sqrt{1 + \gamma_2^2 \text{ctg}^2 \theta}}. \quad (28)$$

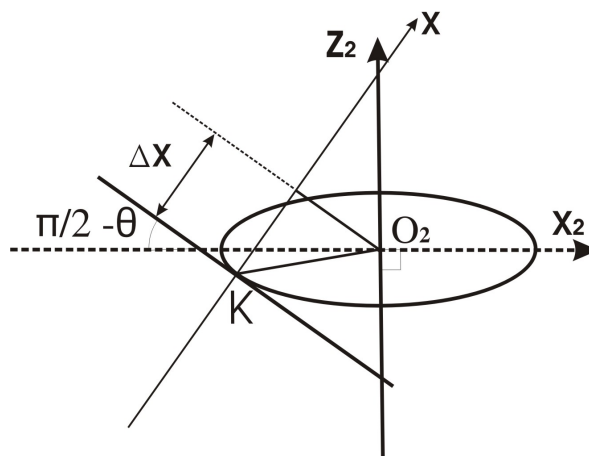


Fig. 15. The fragment of Fig. 14 which is necessary to determine the coordinates of the touching point K in the coordinate system of  $S_2$ .

Turning back from  $(x_2, y_2)$ -coordinate system to  $(x, y)$ -system, in accord with Figs. 14 and 15 one obtains

$$\Delta x = |x_0 \cos \theta - y_0 \sin \theta| = \frac{R_2 \sin \theta}{\gamma_2} \sqrt{1 + \gamma_2^2 \text{ctg}^2 \theta}, \quad (29)$$

and hence we get

$$R_x = R_1 + \frac{R_2 \sin \theta}{\gamma_2} \sqrt{1 + \gamma_2^2 \text{ctg}^2 \theta}. \quad (30)$$

From Fig. 16 one can see that in order to obtain the radius  $R_z$  one should simply replace  $R_1 \rightarrow R_1/\gamma_1$  and  $\pi/2 - \theta \rightarrow \theta$  in expression (30) for the radius  $R_x$ . Then one finds

$$R_z = \frac{R_1}{\gamma_1} + \frac{R_2 \cos \theta}{\gamma_2} \sqrt{1 + \gamma_2^2 \text{tg}^2 \theta}. \quad (31)$$

Finally, substituting Eqs. (23), (30) and (31) into (22) one obtains:

$$V_{exc} = \frac{4\pi}{3} (R_1 + R_2) \left( \frac{R_1}{\gamma_1} + \frac{R_2 \cos \theta}{\gamma_2} \sqrt{1 + \gamma_2^2 \text{tg}^2 \theta} \right) \times \left( R_1 + \frac{R_2 \sin \theta}{\gamma_2} \sqrt{1 + \gamma_2^2 \text{ctg}^2 \theta} \right). \quad (32)$$

Evidently, the expression above precisely recovers the excluded volume of two non-relativistic spheres, i.e. for  $\gamma_1 = \gamma_2 = 1$ . Thus, in contrast to the result of [29] Eq. (32) gives an exact result for the non-relativistic particles. Also one can analytically show that Eq. (32) gives rather good approximation (with the deviation below 10 % from the exact result) also for other extreme cases, when one particle is non-relativistic and another

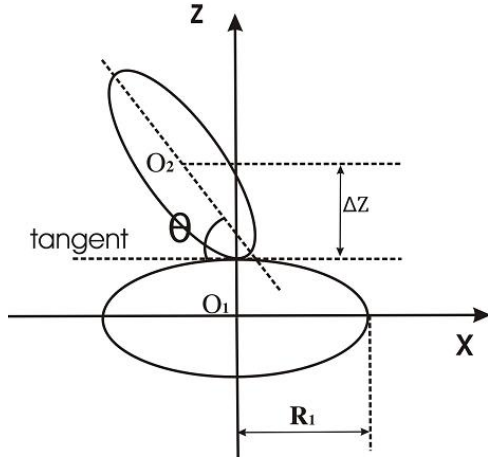


Fig. 16. The projection which is necessary to derive the radius  $R_z$  of the approximate excluded volume (33). Comparing this projection with that one shown in Fig. 14, we find that formally it is necessary to replace  $R_1 \rightarrow R_1/\gamma_1$  and  $\pi/2 - \theta \rightarrow \theta$  in the expression (30) to get the expression for  $R_z$  from that one for  $R_x$ .

particle is ultra-relativistic or when both particles are ultra-relativistic.

Nevertheless, in order to improve (32) further, we symmetrize it with respect to interchange  $1 \leftrightarrow 2$ . Evidently, such a procedure will not break down the above discussed properties of (32). However, a symmetrization of (32) can be done in many possible ways, but numerically we found that the best approximation to an exact result is given by the expression

$$V_{exc}^{rel} = \frac{\pi}{12} (R_z + \tilde{R}_z) \left[ (R_x + R_y)^2 + (\tilde{R}_x + \tilde{R}_y)^2 \right], \quad (33)$$

where the tilded values  $\tilde{R}_a(R_1, R_2, \gamma_1, \gamma_2) = R_a(R_2, R_1, \gamma_2, \gamma_1)$  stand for an interchange  $1 \leftrightarrow 2$  in the expressions for the radii  $R_x$ ,  $R_y$  and  $R_z$  of this Appendix. An expression (33) leads to the following approximate value of the second virial coefficient [29]

$$V_{rel} = \frac{1}{\rho(T, m_1)\rho(T, m_2)} \int \frac{d^3k_1}{(2\pi)^3} \frac{d^3k_2}{(2\pi)^3} V_{exc}^{rel}(k_1, k_2, \Theta_2) \times \exp\left(-\frac{\sqrt{k_1^2 + m_1^2}}{T}\right) \exp\left(-\frac{\sqrt{k_2^2 + m_2^2}}{T}\right), \quad (34)$$

which, evidently, can be analytically integrated over three spherical angles. In Eq. (34) the thermal density of the particle of mass  $m$  at temperature  $T$  is defined as

$$\rho(T, m) = \int \frac{d^3k_1}{(2\pi)^3} \exp\left(-\frac{\sqrt{k_1^2 + m^2}}{T}\right). \quad (35)$$

A comparison between the exact value of the second virial coefficient with the Lorentz contraction accounted

for both particles and the second virial coefficient found from the approximation (33) is depicted in Fig. 17. For such a comparison we choose the worst possible case, i.e. the largest allowed values of the hard-core radii and take the pions since for them the relativistic effects are most important. As one can see from Fig. 17 the approximate expression (33) gives very good description of the pion-pion second virial coefficient. In fact, for temperatures below 180 MeV the relative deviation of the obtained approximation does not exceed 6%. Since the hard-core repulsion provides a small correction (less than 10%) to the system pressure, then the resulting error for the pion pressure generated by the approximation (33) is less than 0.5% for all considered temperatures. The correction to the pressure of heavier hadrons is practically negligible, since the relativistic effects for them are essentially weaker than for pions.

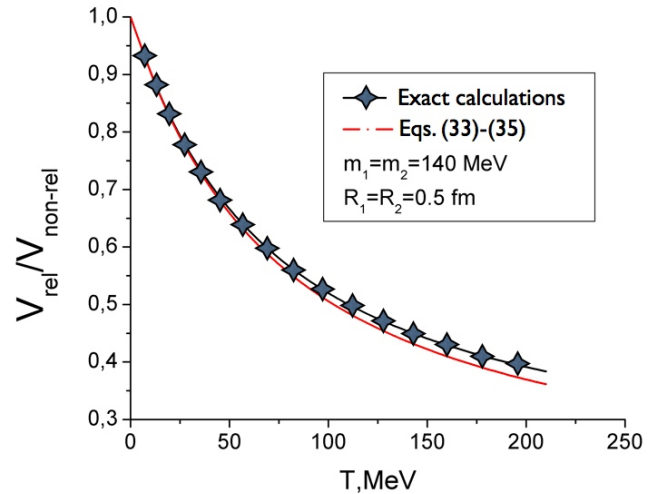


Fig. 17. Temperature dependence of the exact second virial coefficient of two pions (curve with symbols) and its approximation (curve without symbols) given by Eqs. (33)-(35) in the units of non-relativistic excluded volume  $V_{non-rel} = \frac{32}{3}\pi R_1^3$  of two hard spheres of the same radius  $R_1 = R_2 = 0.5$  fm. The comparison is made for pion-pion interaction only, since in this case the effect of Lorentz contraction is strongest.

**Acknowledgments.** We would like to thank A. Andronic for providing an access to well-structured experimental data and A.I. Ivanytskyi, I.N. Mishustin and L.M. Satarov for fruitful discussions. K.A.B. and D.R.O. acknowledge the partial support of the Program ‘On Perspective Fundamental Research in High Energy and Nuclear Physics’ launched by the Section of Nuclear Physics of National Academy of Sciences of Ukraine. The work of

A.S.S. was supported in part by the Russian Foundation for Basic Research, Grant No. 11-02-01538-a.

1. P. Braun-Munzinger, K. Redlich and J. Stachel, arXiv:0304013v1 [nucl-th] and references therein.
2. A. Andronic, P. Braun-Munzinger and J. Stachel, Nucl. Phys. A **772**,167 (2006); arXiv:0511071v3 [nucl-th].
3. A. Andronic, P. Braun-Munzinger and J. Stachel, arXiv:0812.1186v3 [nucl-th].
4. G.D. Yen and M.I. Gorenstein, Phys. Rev. C **59**, 2788 (1999).
5. G.D. Yen, M.I. Gorenstein, W. Greiner and S.N. Yang, Phys. Rev. C **56**, 2210 (1997).
6. A. Andronic, P. Braun-Munzinger, J. Stachel and M. Winn, arXiv:1201.0693v1 [nucl-th].
7. S. Wheaton and J. Cleymans, arXiv:0407174 [hep-ph].
8. L.M. Satarov, M.N. Dmitriev and I.N. Mishustin, Phys. Atom. Nucl. **72**, 1390 (2009).
9. D. Adamova et al. (CERES collaboration), Phys. Rev. Lett. **90**, 022301 (2003); arXiv:0207008 [nucl-ex]; M. Lisa, S. Pratt, R. Soltz and U. Wiedemann, Ann. Rev. Nucl. Part. Sci. **55**, 357 (2005); arXiv:0505014 [nucl-ex].
10. A. Bohr and B. Mottelson, "Nuclear Structure", Vol.1, Benjamin, New York, (1969).
11. P. Braun-Munzinger, I. Heppe and J. Stachel arXiv:9903010v2 [nucl-th].
12. G.D. Yen, M.I. Gorenstein, W. Greiner and S.N. Yang, Phys. Rev. C **56**, 2210 (1997).
13. P. Braun-Munzinger, J. Stachel, J.P. Wesselsa and N. Xu, Phys. Lett. B **344**, 43 (1995); arXiv:9410026 [nucl-th]; Phys. Lett. B **365**, 1 (1996); arXiv:9508020 [nucl-th].
14. J. Cleymans, D. Elliott, A. Keranen and E. Suhonen, Phys. Rev. C **57**, 3319 (1998); arXiv:9711066 [nucl-th]; J. Cleymans, H. Oeschler and K. Redlich, Phys. Rev. C **59**, 1663 (1999); arXiv:809027 [nucl-th].
15. R. Averbeck, R. Holzmann, V. Metag and R.S. Simon, Phys. Rev. C **67**, 024903 (2003); arXiv:0012007 [nucl-ex].
16. P. Braun-Munzinger, I. Heppe and J. Stachel, Phys. Lett. B **465**, 15 (1999); arXiv:9903010 [nucl-th].
17. P. Braun-Munzinger, D. Magestro, K. Redlich and J. Stachel, Phys. Lett. B **518**, 41 (2001); arXiv:0105229 [nucl-th].
18. W. Broniowski, W. Florkowski and M. Michalec, Acta Phys. Polon. B **33**, 761 (2002); arXiv:0106009 [nucl-th]; W. Broniowski and W. Florkowski, Phys. Rev. C **65**, 064905 (2002); arXiv:0112043 [nucl-th].
19. M. Kaneta and N. Xu, arXiv:0405068 [nucl-th].
20. J. Adams et al. (STAR collaboration), Nucl. Phys. A **757**, 102 (2005); arXiv:0501009 [nucl-ex].
21. R. Preghenella, arXiv:1111.7080 [hep-ex].
22. P. Braun-Munzinger and J. Stachel, Nucl. Phys. A **638**, 3c (1998); arXiv:9803015 [nucl-ex].
23. J. Cleymans, K. Redlich, Phys. Rev. Lett. **81**, 5284 (1998), **C 60**, 054908 (1999); J. Cleymans, H. Oeschler, K. Redlich and S. Wheaton, Phys. Rev. **C 73**, 034905 (2006), J. Phys. **G 32**, S165 (2006).
24. K.A. Bugaev, M.I. Gorenstein, H. Stöcker and W. Greiner, Phys. Lett. B **485**, 121 (2000).
25. G. Zeeb, K.A. Bugaev, P.T. Reuter and H. Stöcker, Ukr. J. Phys. **53**, 279 (2008).
26. F. Becattini, M. Gazdzicki, A. Keranen, J. Manninen and R. Stock, Phys. Rev. C **69**, 024905 (2004).
27. A. Dumitru, L. Portugal and D. Zschesche, Phys. Rev. C **73**, 024902 (2006); arXiv:0511084 [nucl-th].
28. K.A. Bugaev, V.K. Petrov and G.M. Zinovjev, Europhys. Lett. **85**, 22002 (2009); arXiv:0801.4869v2 [hep-ph] and references therein.
29. K.A. Bugaev, Nucl. Phys. A **807**, 251 (2008); arXiv:1012.3400 [nucl-th].
30. R.A. Ritchie, M.I. Gorenstein and H.G. Miller, Z. Phys. C **75** 2002 (1997).
31. R.K. Pathria, "Statistical Mechanics", Pergamon Press, Oxford (1972).
32. K.A. Bugaev, Phys. Rev. C **76**, 014903 (2007); Phys. Atom. Nucl. **71**, 1615 (2008);
33. A.I. Ivanytskyi, Nucl. Phys. A **880**, 12 (2012).
34. K.A. Bugaev, V.K. Petrov and G. M. Zinovjev, Phys. Part. Nucl. Lett. **9**, 397 (2012).
35. K.A. Bugaev and G. M. Zinovjev, Nucl. Phys. A **848**, (2010); K.A. Bugaev, Phys. Part. Nucl. Lett. **8**, 907 (2011).
36. K.A. Bugaev, A.I. Ivanytskyi, E.G. Nikonov, V.K. Petrov, A.S. Sorin and G.M. Zinovjev, Phys. Atom. Nucl. **75**, 1 (2012).
37. M.E. Fisher, Physics **3**, 255 (1967).
38. K. A. Bugaev, M. I. Gorenstein, I. N. Mishustin and W. Greiner, Phys. Rev. C **62**, 044320 (2000); Phys. Lett. B **498**, 144 (2001).
39. S. K. Tiwari, P. K. Srivastava and C. P. Singh, Phys. Rev. C **85**, 014908 (2012).
40. M. Gazdzicki and M. I. Gorenstein, Acta Phys. Polon. B **30**, 2705 (1999).
41. M. I. Gorenstein, M. Gazdzicki and K. A. Bugaev, Phys. Lett. B **567**, 175 (2003).
42. M. Gazdzicki, M. I. Gorenstein and P. Seyboth, Acta Phys. Polon. B **42**, 307 (2011).

Received 14.08.12